Ulaby, F. T., et al., 1981. *Microwave Remote Sensing: Active and Passive. I – Microwave Remote Sensing Fundamentals and Radiometry.* Reading, MA: Addison-Wesley.
Ulaby, F. T., et al., 1982. *Microwave Remote Sensing: Active and Passive. II – Radar Remote Sensing and Surface Scattering and Emission Theory.* Reading, MA: Addison-Wesley.
Wentz, F. J., 1997. A well calibrated ocean algorithm for SSM/I. *Journal of Geophysical Research*, **102**, 8703–8718.

Cross-references

Coastal Ecosystems
Fisheries
Global Climate Observing System
Ocean Data Telemetry
Ocean Internal Waves
Ocean Measurements and Applications, Ocean Color
Ocean Modeling and Data Assimilation
Sea Ice Concentration and Extent
Sea Surface Temperature
Sea Surface Salinity
Sea Surface Wind/Stress Vector

OCEAN-ATMOSPHERE WATER FLUX AND EVAPORATION

W. Timothy Liu and Xiaosu Xie
Jet Propulsion Laboratory, California Institute of Technology, Pasadena, CA, USA

Definition

The ocean–atmosphere water exchange is the difference between evaporation and precipitation at the surface of the ocean. Evaporation is the turbulent transport of water vapor from ocean to the atmosphere. Precipitation is the return of water to the ocean from the atmosphere in the form of rain and snow.

Introduction

The equation of water conservation in the atmospheric column is

$$\frac{\partial W}{\partial t} + \cdot\boldsymbol{\Theta} = \mathbf{E} - \mathbf{P} = \mathbf{F} \tag{1}$$

where

$$\boldsymbol{\Theta} = \int_0^{p_s} q\mathbf{u}dp \tag{2}$$

is the moisture transport integrated over the depth of the atmosphere, and

$$W = \frac{1}{g}\int_0^{p_s} qdp \tag{3}$$

is the precipitable water or column-integrated water vapor. In these equations, p is the pressure, p_s is the pressure at the surface, and q and **u** are the specific humidity and wind vector at a certain level. Bold symbols represent vector quantities. F is the freshwater exchange between the ocean and the atmosphere and is the difference between evaporation (E) and precipitation (P) at the surface. The first term is the change of storage. For periods longer than a few days, it is negligible, and there is a balance between the divergence of the transport ($\nabla \cdot \boldsymbol{\Theta}$) and the surface flux. The balance gives rise to two ways of estimating the fresh water flux. One is to measure E and P separately; the other is to estimate $\boldsymbol{\Theta}$.

The first method, through the small turbulent-scale processes, has been called the "supply side" estimation; the water is supplied by transport from the ocean. The second method has been called the "demand side" estimation; the large-scale atmospheric circulation demands the water flux from the ocean (WCRP, 1983). One of the most advanced statistical techniques, support vector regression (SVR), has been used to retrieve surface specific humidity (q), E, and $\boldsymbol{\Theta}$, from space-based data.

The scientific need of the flux is presented in section Significance. Space-based estimations of q and E are described in section Bulk Parameterization: The Supply Side. The validation of the water flux is difficult because of the lack of credible direct measurements. The conservation principles post constraints of the accuracy of these fluxes. The space-based estimation of $\nabla \cdot \boldsymbol{\Theta}$ as water flux is described in section Divergence of Moisture Transport: The Demand Side, which includes the validation through mass conservation of global ocean and the continent of South America. In turn, $\nabla \cdot \boldsymbol{\Theta}$ is used as a constraint to the accuracy of E retrieval (Equation 1) in section Marine Atmosphere Water Conservation. The feasibility of applying further constraints is explored in section Ocean Heat and Surface Salinity Conservation.

There are many programs to produce P (e.g., Huffman et al., 1997; Adler et al., 2003; Joyce et al., 2004). The Tropical Rainfall Measuring Mission (TRMM, Kummerow et al., 2000) measures rainfall between 38° latitude north and south of the equator and has provided important calibration of P since 1998. The Global Precipitation Mission (GPM) will extend the coverage to extratropical regions, with increased sensitivity and accuracy. See Rainfall, by R. Ferraro, in this book for further discussion.

Significance

Water is the essential element for life. Over 70 % of the Earth's surface is covered by the ocean, which forms the largest reservoir of water on Earth. The never-ending recycling process in which a small fraction of water is continuously removed from the ocean as excess evaporation over precipitation into the atmosphere, redistributed through atmospheric circulation, deposited as excess precipitation over evaporation on land, and returned to the ocean as river discharge, is critical to the existence of human life and the variability of weather and climate.

With their high specific heat and large thermal inertia, the oceans are also the largest reservoir of heat and the flywheel of the global heat engine. Since water has high latent heat, evaporation is also an efficient way to transfer the energy. Besides releasing latent heat to the atmosphere, the water evaporated from the surface forms clouds, which absorb and reflect radiation. Water vapor is also an important greenhouse gas, which absorbs more long-wave radiation emitted by Earth than the short-wave radiation from the Sun. Redistribution of clouds and water vapor changes the Earth's radiation balance.

The hypothesis of the amplification of water cycle resulted from global warming, which essentially states that wet places get wetter and dry places get dryer, is a typical problem joining the water and energy balances. Increase in global mean precipitation down to the surface has to be balanced by equal amount of evaporation from the surface to conserve water in the atmosphere. Increase in latent heat from the surface carried by evaporation requires increase in long-wave radiation down to the surface; any imbalance will result in climate changes.

The differential heating of the atmosphere by the ocean fuels atmospheric circulation, which in turn drives ocean currents. Both wind and current transport and redistribute heat and greenhouse gases. Adding heat and water changes density of air and seawater. The heat and water fluxes, therefore, change both the baroclinicity and stability (horizontal and vertical density gradients) of the atmosphere and the ocean. These in turn modify the shears of wind and current.

Bulk parameterization: the supply side

Most productions of space-based evaporation data sets in the past were based on bulk parameterization. Latent heat flux (LH) is related to E by the nearly constant value of latent heat of vaporization (L): $LH = L \times E$. LH, rather than E, is used in many of the past studies. The two parameters are used interchangeably in this entry, and our discussion on E applies equally to LH.

The computation of E by the bulk parameterization requires sea surface temperature (SST), wind speed (u), and q.

$$E = C_E \rho u (q_s - q) \tag{4}$$

where C_E is the transfer coefficient and ρ is the surface air density. q_s is usually taken to be the saturation humidity at SST multiplied by a factor of 0.98 to account for the effect of salt in the water. u and q should be measured in the atmospheric surface (constant flux) layer, usually taken at a reference level of 10 m. Over the ocean, u and SST have been measured from space, but not q. A method of estimating E using satellite data was demonstrated by Liu and Niiler (1984), based on an empirical relation between W and q on a monthly timescale over the global ocean (Liu, 1986). The physical rationale is that the vertical distribution of water vapor through the whole depth of the atmosphere is coherent for periods longer than a week (Liu et al., 1991). The relation has been scrutinized in a number of studies and many variations of this method have been proposed to improve on the estimation (see Liu and Katsaros, 2001, for a review of earlier studies). Modification of this method by including additional estimators has been proposed (e.g., Wagner et al., 1990; Cresswell et al., 1991; Miller and Katsaros, 1991; Chou et al., 1995) with various degrees of improvement. Recently, neural network has also been used to mitigate the nonlinearity problem in deriving q (Jones et al., 1999; Bourras et al., 2002; Roberts et al., 2010). Algorithms to retrieve q from brightness temperatures (BT) measured by microwave radiometers were developed and improvements were demonstrated (e.g., Schulz et al., 1997; Schlüssel et al., 1995; Jackson et al., 2009). Yu and Weller (2007) have combined space-based observations with model output. Figure 1 shows the validation of q derived from BT measured by the Advanced Microwave Scanning Radiometer – Earth Observing System (AMSR-E) through a statistical model built on SVR. The model outputs are compared with coincident q measured at buoys. For the year of 2008, 30,000 buoy data were randomly selected for validation. The mean and root mean square (rms) differences are 0.05 and 1.05 g/kg, respectively. The rms difference is only 5 % of the range of 20 g/kg and the statistical model appears to be successful. However, E depends on $\Delta q = q_s - q$, which is the small difference between the two large terms (q_s and q), and a small percentage error in q may still cause a large error in Δq and E.

Liu (1990) suggested and demonstrated two potential ways to improve E retrieval from satellite data. The first is to incorporate information on vertical distribution of humidity given by atmospheric sounders. Jackson et al. (2009) have recently adopted this suggestion. The other is to retrieve E directly from the radiances, since all the bulk parameters used in the traditional method could be derived from radiances measured by a microwave radiometer. The direct retrieval method may improve accuracy in two ways. The first is the use of a single CE to derive E (in training the statistical model). The second is to mitigate the magnification of error caused by multiplying inaccurate measurement of wind speed with inaccurate measurements of humidity (q and q_s) in the bulk formula.

Figure 2 compares the uncertainties of two sets of LH derived from the two methods. For the first set, SST and u from AMSR-E produced by Remote Sensing System (Wentz and Meissner, 2000) are used with q derived from AMSR-E BT (same as those in Figure 1). The second set is the output of a statistical model built on SVR, predicting E from the 12-channel AMSR-E BT. A total of 30,000 randomly selected LH computed from three groups of buoy data in 2008 are used in the validation exercise. Direct retrieval of daily mean values reduces the rms difference from 77 W/m^2 of the bulk parameterization method to 38 W/m^2. This is equivalent to a reduction from 19 % to 9.7 % of the dynamic range of 400 W/m^2.

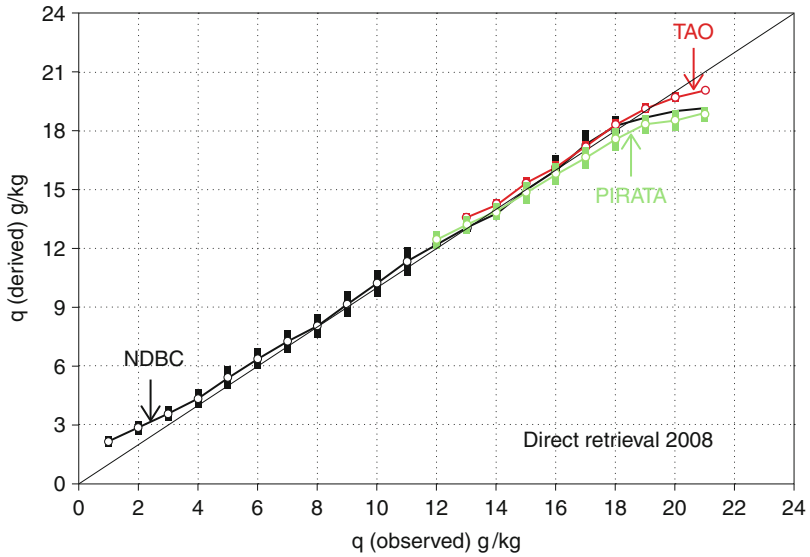

Ocean-Atmosphere Water Flux and Evaporation, Figure 1 Bin-average of near surface specific humidity (q) derived from the statistical model compared with values measured at three groups of buoys. Standard deviation is superimposed on each bin-average as error bar.

The available E (or LH) products and the bulk parameters used to derive them exhibit substantial differences even for monthly means (e.g., Brunke et al., 2002; Bourras, 2006; Smith et al., 2011; Santorelli et al., 2011). The results of our direct retrieval depend on the mix of training data (buoy and ship measurements and NWP products). The conservation principle Equation 1 and the demand-side evaluation may serve as an effective way to evaluate current E products.

Divergence of moisture transport: the demand side

The computation of $\boldsymbol{\Theta}$, as defined in Equation 2, requires the vertical profile of q and $\mathbf{u}$, which are not measured by space-based sensors with sufficient resolution. $\boldsymbol{\Theta}$ can be viewed as the column of water vapor W advected by an effective velocity $\mathbf{u_e}$, so that $\mathbf{u_e}=\boldsymbol{\Theta}/W$, and $\mathbf{u_e}$ is the depth-averaged wind velocity weighted by humidity. W has been derived from microwave radiometer measurements with good accuracy. Methods were developed to relate $\mathbf{u_e}$ to the equivalent neutral wind measured by scatterometers, $\mathbf{u_s}$, based on polynomial regression (Liu, 1993) and neural network (Liu and Tang, 2005). Xie et al. (2008) added cloud-drift winds at 850 mb to $\mathbf{u_s}$ and used SVR instead of neural network. The scatterometer measurement and the cloud-drift winds represent ocean surface stress and free-stream velocity, respectively. Xie et al. (2008) showed that $\boldsymbol{\Theta}$ derived from their statistical model agrees with $\boldsymbol{\Theta}$ derived from 90 rawinsonde stations from synoptic to seasonal timescales and from equatorial to polar oceans. Hilburn (2010) found very good agreement between this data set and data computed from Modern Era Retrospective-analysis for Research and Applications (MERRA) over the global ocean. MERRA is a NASA atmospheric reanalysis using a major new version of the Goddard Earth System Data Assimilation System (Rienecker et al., 2011). Figure 3 shows that, for a total of 26,000 pairs randomly selected data, 2/3 from rawinsonde and 1/3 from the reanalysis, the rms difference is 57.5 kg/m/s and the correlation coefficient is 0.95 for zonal component, and 49.7 kg/m/s and 0.89 for meridional component, for a range of approximately −600 to +600 kg/m/s.

Validation of our space-based estimation of $\nabla\cdot\boldsymbol{\Theta}$(as F) was achieved through mass balance of oceans and continents, using data of the Gravity Recovery and Climate Experiment (GRACE), which is a geodesy mission to measure Earth's gravity field. The variations of the gravity field are largely the results of the change of water storage. The air-sea water flux given by $\nabla\cdot\boldsymbol{\Theta}$ integrated over all ocean area, together with river discharge (R) from all continents, should balance the rate of mass change (∂M/∂t) of all oceans:

$$\iint \frac{\partial M}{\partial t} = \int R - \iint \cdot\boldsymbol{\Theta} \tag{5}$$

where $\int$ and $\iint$ represent line and area integrals, respectively. Figure 4 shows that monthly rate of mass change ($-\partial$M/∂t), measured by GRACE, integrated over all oceans, agrees in magnitude and in phase with $\nabla\cdot\boldsymbol{\Theta}$, derived from the statistical model of Xie et al. (2008) integrated over all ocean areas minus the line integral of R over all coastlines. The difference between $-\int\int\partial M/\partial t$ and $\int\int\nabla\cdot\boldsymbol{\Theta}-\int R$ has a mean of 2.1×10^8 kg/s and a standard deviation of 2.6×10^8 kg/s. The standard

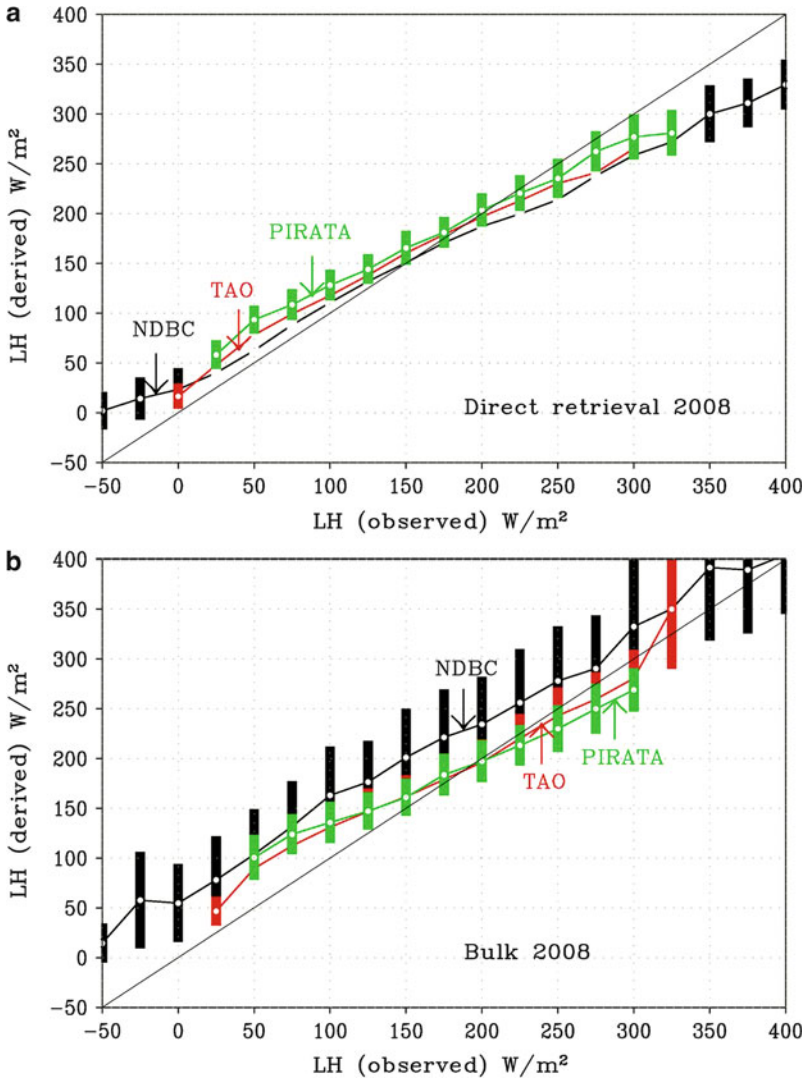

Ocean-Atmosphere Water Flux and Evaporation, Figure 2 Bin-average of LH derived directly from the satellite measured radiances (**a**), and computed from bulk parameters (**b**), compared with coincident measurements at three groups of buoys. Standard deviation is superimposed on each bin-average as error bar.

deviation is 18 % of the peak-to-peak variation of 12 $\times$ 10^8 kg/s. The uncertainties in time varying river discharge and ice melt contribute to a large part of error. In the long term, mass is conserved, and the first term in Equation 5 is negligible. The total ocean surface water flux should balance the total water discharge from continent to ocean. The $\int\int \nabla \cdot \mathbf{\Theta}$ 4 year mean of 10.6 cm/year, computed from outputs of the statistical model, is lower than the climatological value of 12 cm/year given in textbook published 36 years ago (Budyko, 1974) and higher than the climatological river discharge of 8.6 cm/year (Dai and Trenberth, 2002). Large and Yeager (2009) compiled available E and P to give an annual mean of 11 cm/yr. There are, in general, 20 % uncertainties of these hydrologic balances over global ocean (Figure 4).

Based on Green's Theorem, the areal integral of the flux divergence should balance the line integral of flux out of the boundary. The last term of Equation 5 should equal to total water vapor across the coastlines of all continents. Another example of validation by the conservation principle is given by Liu et al. (2006). They first demonstrated the continental water balance in South America (Figure 5). With climatological river discharge ($\int$R) removed from $\int\mathbf{\Theta}$ across the entire continental coastline, the residue agrees, both in phase and in magnitude, with monthly rate of mass change ($\int\int\partial$M/∂t). The standard deviation of the difference between $\int\int\partial$M/∂t and moisture flux-river discharge is 0.9 $\times$ 10^8 kg/s, which is 7 % of the peak-to-peak variation of 13 $\times$ 10^8kg/s.

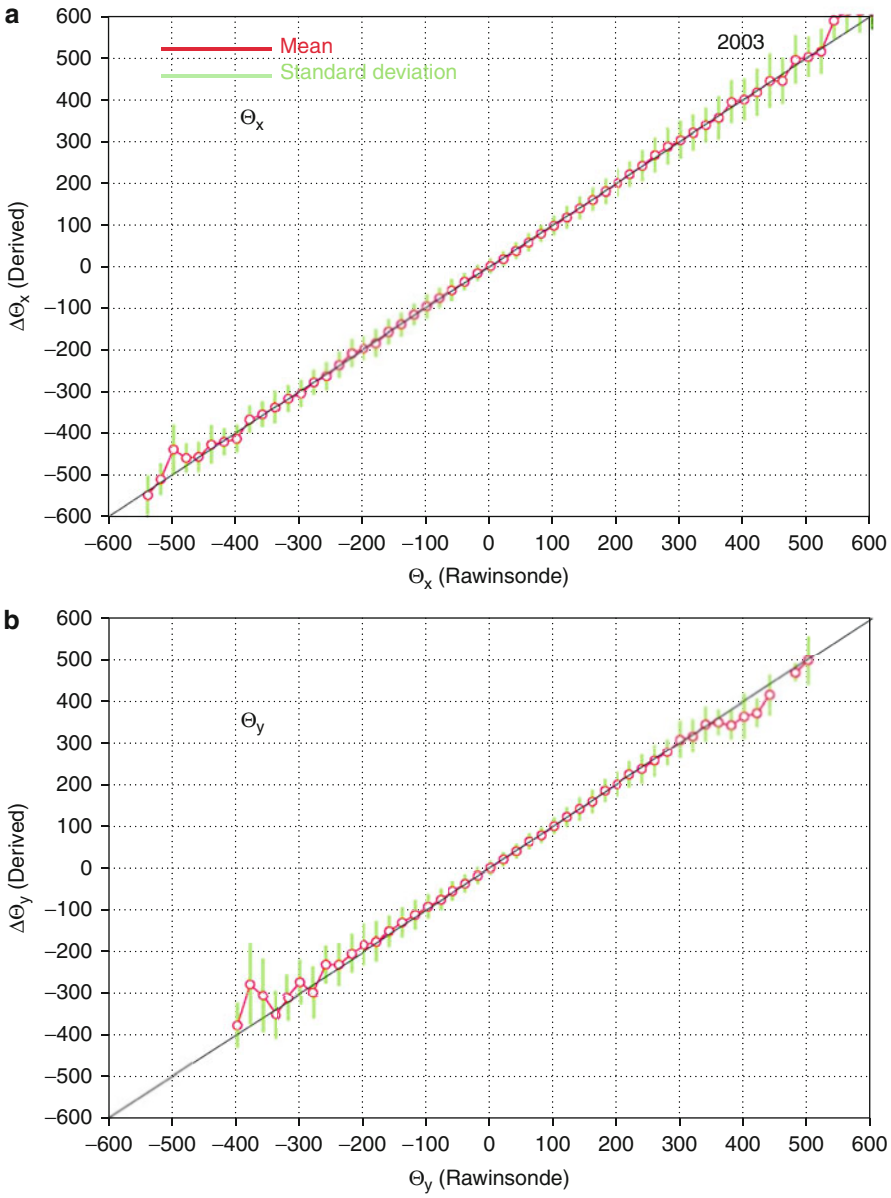

Ocean-Atmosphere Water Flux and Evaporation, Figure 3 Bin-averaged zonal component (**a**) and meridional component (**b**) of integrated moisture transport ($\boldsymbol{\Theta}$), derived from satellite data, compared with coincident data computed from rawinsondes.

Marine atmosphere water conservation

The two flux products should agree with the conservation principle (Equation 1). As an example, the 3 year averages of $\nabla \cdot \boldsymbol{\Theta}$ and E-P are shown in Figure 6. In this example, P is based on TRMM merged data product 3B42, and E is from our direct retrieval from BT. There are general agreements in the magnitude and geographical distribution, but differences in the details. Away from coastal regions, the supply side is larger than the demand side in the tropical southeastern Pacific, tropical south Atlantic, and a region from the Somali coast extending into the northern Arabian Sea. The demand side is larger than the supply side in the warm pool of the western tropical Pacific and under the Intertropical Convergence Zone (ITCZ). Two operational E products : the Hamburg Ocean Atmosphere Parameters and Fluxes from Satellite Data (HOAPS 3, Andersson et al., 2010) and the Objectively Analyzed air-sea Fluxes (OAFlux) (Yu and Weller, 2007), combined with the same TRMM precipitation are also shown as comparison.

The differences between supply and demand side may reveal regional hydrodynamics. E is the air-sea

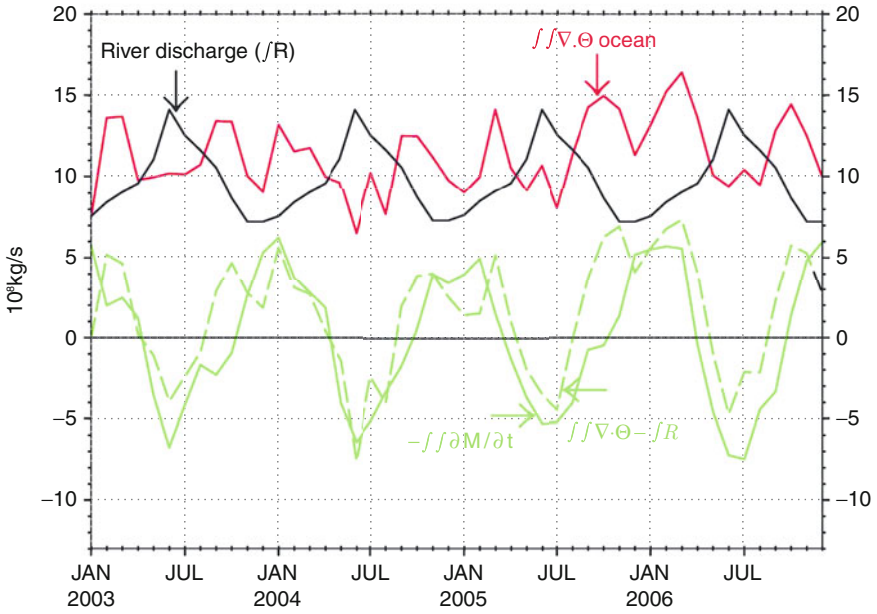

Ocean-Atmosphere Water Flux and Evaporation, Figure 4 Annual variation of hydrologic parameters integrated over global oceans.

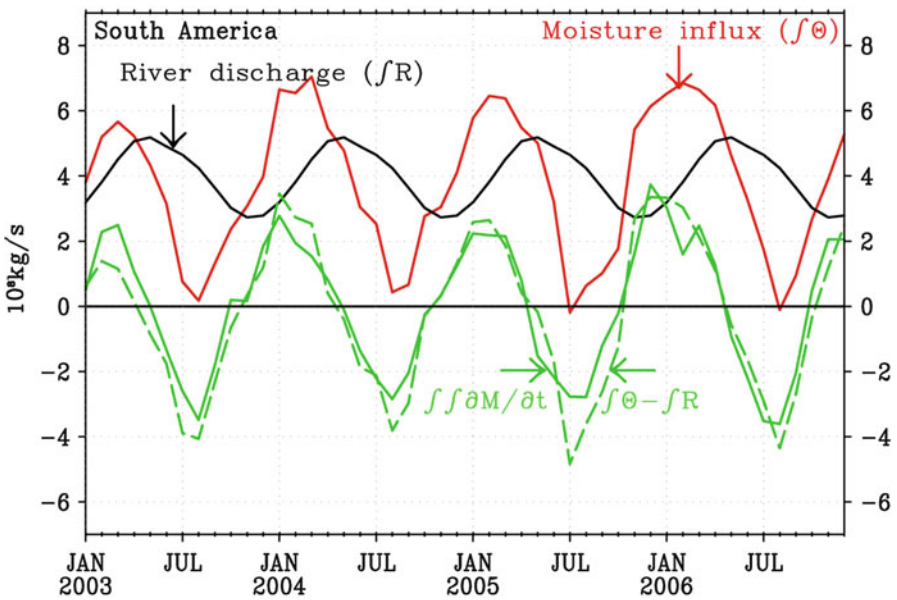

Ocean-Atmosphere Water Flux and Evaporation, Figure 5 Annual variation of hydrologic parameters over South America: mass change rate $\int\int\partial M/\partial t$ (*solid green line*), climatological river discharge $\int R$ (*solid black line*), total moisture transport across coastline into the continent $\int\boldsymbol{\Theta}$ (*red line*), and $\int\boldsymbol{\Theta}$-$\int R$ (*dashed green line*).

exchange of water vapor by turbulence; the small-scale turbulence is largely independent of factors governing large-scale atmospheric circulation (e.g., baroclinicity, Coriolis force, pressure gradient force, cloud entrainment), while $\boldsymbol{\Theta}$ is not as sensitive as E to small-scale ocean processes.

Ocean heat and surface salinity conservation

Evaporative cooling is a major variable component of ocean surface heat balance. The LH has been combined with sensible heat flux (SH) and radiative fluxes to provide the net surface thermal forcing of the ocean (Liu and Gautier, 1990; Liu et al., 1994).

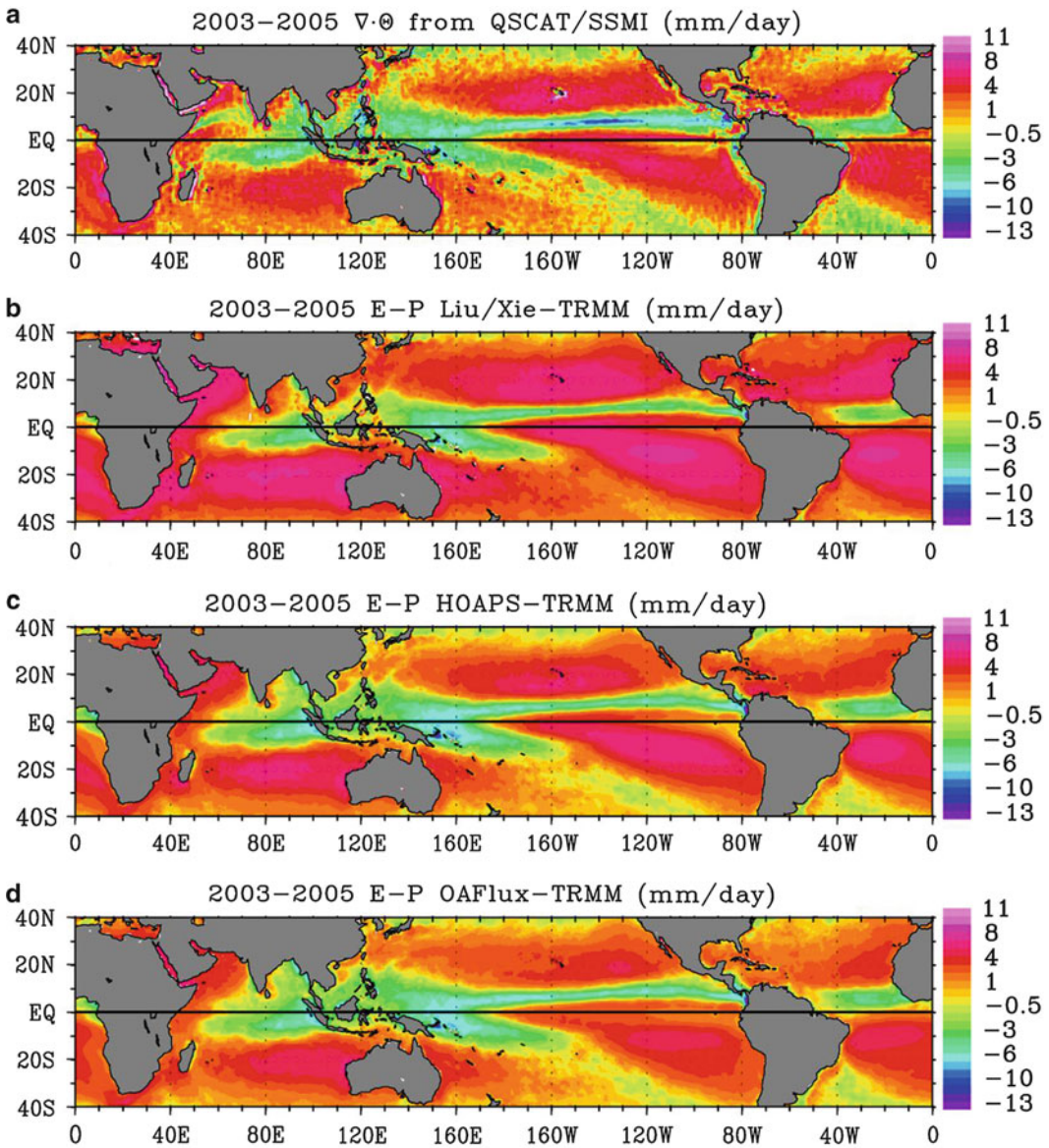

Ocean-Atmosphere Water Flux and Evaporation, Figure 6 Three year (2003–2005) annual mean distribution of (**a**) the divergence of integrated moisture transport, (**b**) evaporation-precipitation derived from AMSR-E and TRMM, (**c**) and (**d**) are the same as (**b**) except for evaporation from HOAPS 3 and OAFlux.

The meridional heat transport (MHT) at a latitude θ is derived by integrating from θ to θ_0 across the width of an ocean basin (x_1 to x_2), the rate of heat content changes subtracting the net surface heat flux,

$$\mathrm{MHT}(\theta) = \int_{\theta}^{\theta_0} \int_{x_1}^{x_2} \left(\frac{\partial \mathrm{H}}{\partial \mathrm{t}} - \mathrm{SW} + \mathrm{LW} + \mathrm{LH} + \mathrm{SH} \right) dxdy \tag{6}$$

where H is the heat content, SW is the net incoming short-wave radiation flux, and LW is the net outgoing long-wave radiation flux.

The northern end of the ocean basin (θ_0) is treated as conclosed by land. The long term mean meridional heat transport of the major ocean basins have been estimated from the ocean surface fluxes (WCRP, 1982). With recent intense effort to measure the meridional overturning current and the feasibility of measuring H by Argo floats, GRACE, and radar altimeter, we may even examine the temporal variation of the meridional heat transport as a constraint to the LH.

There are large uncertainties in long-term annual mean of MHT compiled in past studies, including those derived from surface flux climatology and from oceanographic

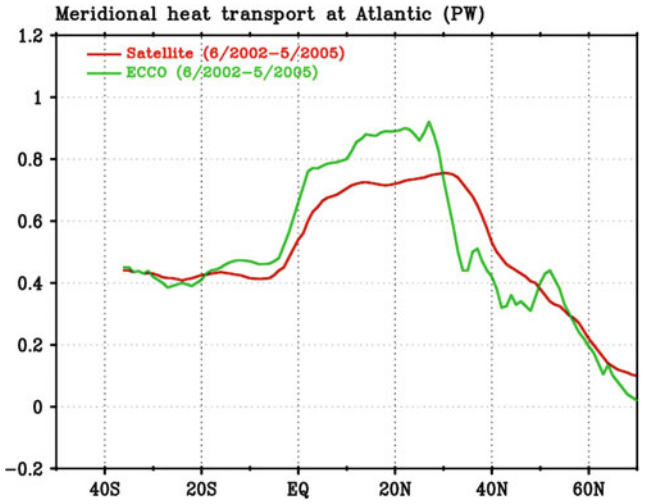

Ocean-Atmosphere Water Flux and Evaporation, Figure 7 Comparison of annual mean MHT at the Atlantic as a function of latitude. *Red curve* is calculated using the surface heat balance from satellite observations (SW and LW from the Surface Radiation Budget (SRB), LH and SH from AMSR-E). The *green curve* is computed from ECCO data.

measurements. Figure 7 shows that the MHT computed from our space-based surface heat flux (red line) is lower than those from the simulation of the Estimating the Circulation and Climate of the Ocean (ECCO) model (green line, Fukumori, 2002) between the equator and 30 °N and higher than ECCO between 30 °N and 50 °N. It agrees with ECCO surprisingly well south of the equator.

The equation of water balance in the upper ocean is

$$\frac{h_0}{S_0}\left(\frac{\partial S}{\partial t} + \mathbf{V}.\mathrm{S}\right) = \mathrm{E} - \mathrm{P} \qquad (7)$$

where V is current and S is salinity in the surface mixed layer with average depth h_0 and average salinity S_0. Salinity measurements have advanced by the Argo floats and space-based sensors of Aquarius and the Soil Moisture and Ocean Salinity Mission (SMOS). The current velocity has been derived from the displacements of drifters with drogues centered at 15 m depth (Niiler, 2001). Ocean surface currents are also provided by the Ocean Surface Currents Analysis-Real-time (OSCAR) program, using a combination of scatterometer and altimeter data (Lagerloef et al., 1999), at a 5 day and 1° resolution between 70 °S to 70 °N. The ocean surface salinity balance can also be used to put constraints on the accuracy of F. The first term represents the change of storage could be neglected in the long-term mean.

Figure 8 shows the distribution of the surface flux agrees with the distribution of salinity advection in the general features, using Argo data for the 11 year mean and using Aquarius for the 1 year mean.

Summary

There have been continuous endeavors to estimate E and LH over global oceans using satellite data and based on bulk parameterization of turbulence transport, since Liu and Niiler (1984) successfully estimated the flux by introducing an empirical relation between monthly W and q. With some improvement in this "supply side" approach, a number of data sets have been operationally produced in the past two decades, but large differences among these data sets and between products from satellite data and from reanalysis of operational weather prediction remain (e.g., Curry et al., 2004). We have introduced a new method of direct retrieval of E and LH from the radiances measured by microwave radiometers, which improves the random error of the daily value of LH to 10 % of the dynamic range, as compared with the 19 % error using the methods we pioneered 30 years ago of computing the fluxes from bulk parameters derived from the same radiances.

Evaluations to find the optimal flux product are difficult because of the lack of credible standards (e.g., extensive direct flux measurement). One good constraint to the uncertainties is the closure of the atmospheric water budget, which dictates that E-P should balance $\nabla \cdot \boldsymbol{\Theta}$. The "demand side" approach of estimating $\boldsymbol{\Theta}$ and $\nabla \cdot \boldsymbol{\Theta}$ from satellite data serves not only as a credible way to evaluate traditional "supply side" flux products but also to provide the ocean freshwater exchange as a whole, without the need of securing precipitation data separately. The $\boldsymbol{\Theta}$ data have been extensively tested in comparison with all available rawinsonde data and products of numerical models. The water flux data, as $\nabla \cdot \boldsymbol{\Theta}$, are also validated through mass conservation using data from GRACE and river discharge climatology; the validation study shows 20 % uncertainties of the seasonal water balance. The feasibility of using upper ocean heat and salinity conservations is also demonstrated with very preliminary results.

There is still much room left for improvement in estimating water flux over global ocean. The new space-based data products, with better spatial and temporal resolution, have many ongoing scientific applications.

Acknowledgment

This report was prepared at the Jet Propulsion Laboratory (JPL), California Institute of Technology, under contract with the National Aeronautics and Space Administration (NASA). The Precipitation Measuring Mission, NASA Energy and Water Studies, and the Physical Oceanography Program (through the Ocean Surface Salinity and the Ocean Surface Vector Wind Science Teams) jointly supported this effort. Open data access is provided at http://airsea.jpl.nasa.gov/seaflux/water-exchange.html, by the Climate Science Center of JPL as its strategic planning.

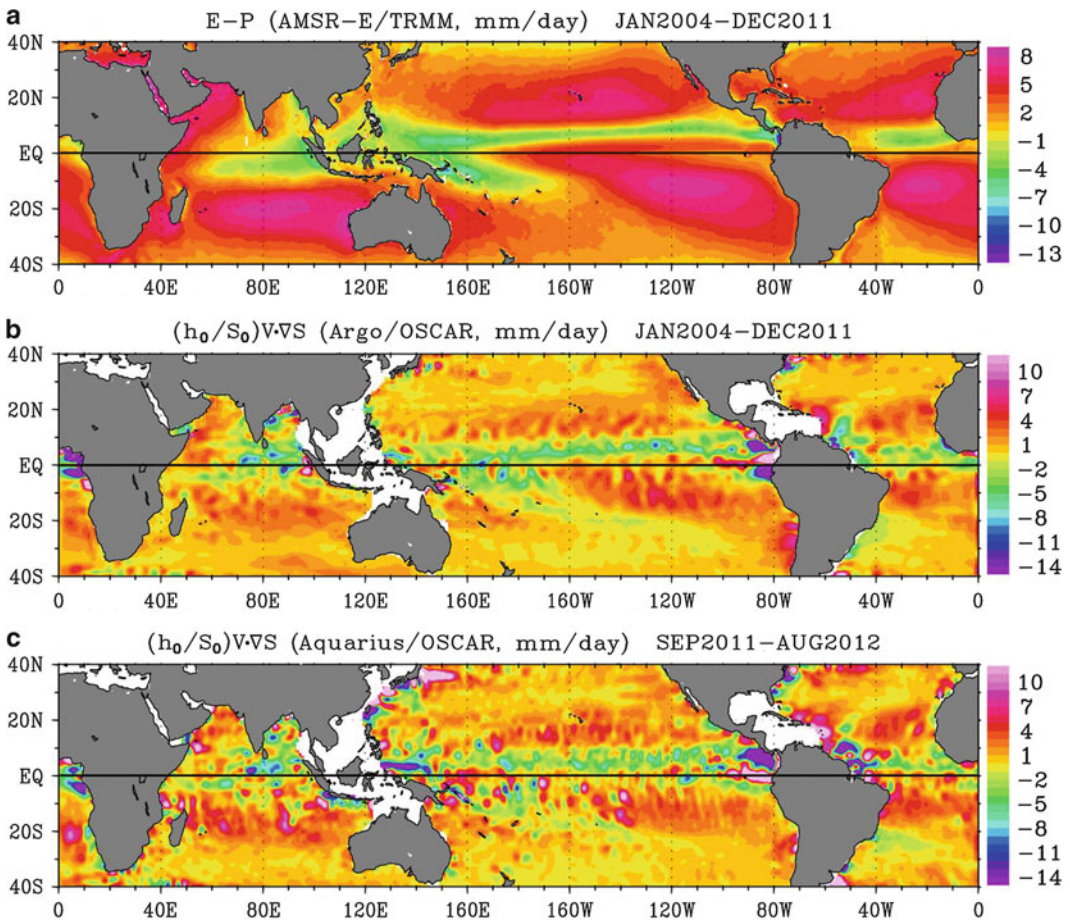

Ocean-Atmosphere Water Flux and Evaporation, Figure 8 (**a**) E-P calculated from AMSR-E and TRMM, (**b**) salinity advection estimated using Argo and OSCAR data, averaged from 2004 to 2011, and (**c**) salinity advection from Aquarius and OSCAR data averaged from September 2011 to August 2012.

Bibliography

Adler, R. F., Huffman, G. J., Chang, A., Ferraro, R., Xie, P., Janowiak, J., Rudolf, B., Schneider, U., Curtis, S., Bolvin, D., Gruber, A., Susskind, J., Arkin, P., and Nelkin, E., 2003. The version-2 global precipitation climatology project (GPCP) monthly precipitation analysis (1979-present). *Journal of Hydrometeorology*, **4**, 1147–1167.

Andersson, A., Fennig, K., Klepp, C., Bakan, S., Grassl, H., and Schulz, J., 2010. The Hamburg Ocean atmosphere parameters and fluxes from satellite data - HOAPS-3. *Earth System Science Data*, **2**, 215–234, doi:10.5194/essd-2-215-2010.

Bourras, D., 2006. Comparison of five satellite-derived latent heat flux products to moored buoy data. *Journal of Climate*, **19**, 6291–6313.

Bourras, D., Eymard, L., and Liu, W. T., 2002. A neural network to estimate the latent heat flux over oceans from satellite observations. *International Journal of Remote Sensing*, **23**, 2405–2423.

Brunke, M. A., Zeng, X., and Anderson, S., 2002. Uncertainties in sea surface turbulent flux algorithms and data sets. *Journal of Geophysical Research*, **107**(C10), 3141, doi:10.1029/2001JC000992.

Budyko, M. I., 1974. *Climate and Life*. New York: Academic.

Chou, S. H., Atlas, R. M., and Ardizzone, J., 1995. Estimates of surface humidity and latent heat fluxes over oceans from SSM/I data. *Monthly Weather Review*, **123**, 2405–2435.

Cresswell, S., Ruprecht, E., and Simmer, C., 1991. Latent heat flux over the North Atlantic Ocean-a case study. *Journal of Applied Meteorology*, **30**, 1627–1635.

Curry, J. A., et al., 2004. Seaflux. *Bulletin of the American Meteorological Society*, **85**, 409–419.

Dai, A., and Trenberth, K. E., 2002. Estimates of freshwater discharge from continents: latitudinal and seasonal variations. *Journal of Hydrometeorology*, **3**, 660–687.

Fukumori, I., 2002. A partitioned Kalman filter and smoother. *Monthly Weather Review*, **130**, 1370–1383.

Hilburn, K. A., 2010. Intercomparison of water vapor transport datasets. *Presented at 17th Conference on Satellite Meteorology and Oceanography and 17th Conference on Air-Sea Interaction*, Annapolis, MD.

Huffman, G. J., Adler, R. F., Arkin, P. A., Chang, A., Ferraro, R., Gruber, A., Janowiak, J. J., Joyce, R. J., McNab, A., Rudolf, B., Schneider, U., and Xie, P., 1997. The global precipitation climatology project (GPCP) combined precipitation data set. *Bulletin of the American Meteorological Society*, **78**, 5–20.

Jackson, D. L., Wick, G. A., and Robinson, F. R., 2009. Improved multisensor approach to satellite-retrieved near-surface specific humidity observations. *Journal of Geophysical Research*, **114**, D16303, doi:10.1029/2008JD011341.

Jones, C., Peterson, P., and Gautier, C., 1999. A new method for deriving ocean surface specific humidity and air temperature: an artificial neural network approach. *Journal of Applied Meteorology*, **38**, 1229–1245.

Joyce, R. J., Janowiak, J. E., Arkin, P. A., and Xie, P., 2004. CMORPH: a method that produces global precipitation estimates from passive microwave and infrared data at high spatial and temporal resolution. *Journal of Hydrometeorology*, **5**, 487–503.

Kummerow, C., et al., 2000. The status of the tropical rainfall measuring mission (TRMM) after two years in orbit. *Journal of Applied Meteorology*, **39**, 1965–1982.

Lagerloef, G. S. E., Mitchum, G., Lukas, R., and Niiler, P., 1999. Tropical Pacific near-surface currents estimated from altimeter, wind and drifter data. *Journal of Geophysical Research*, **104**, 23,313–23,326.

Large, W.G., Yeager, S.G., 2009. The global ciimatology of an internannually varying air-sea flux data set. Glim. Dyn, 33, 341–364.

Liu, W. T., 1986. Statistical relation between monthly precipitable water and surface-level humidity over global oceans. *Monthly Weather Review*, **114**, 1591–1602.

Liu, W. T., 1990. Remote sensing of surface turbulence flux. In Geenaert, G. L., and Plant, W. J. (eds.), *Surface Waves and Fluxes*. Dordrecht: Kluwer, Vol. II, pp. 293–309. Chapter 16.

Liu, W. T., 1993. Ocean surface evaporation. In Gurney, R. J., Foster, J., and Parkinson, C. (eds.), *Atlas of Satellite Observations Related to Global Change*. Cambridge: Cambridge University Press, pp. 265–278.

Liu, W. T., and Gautier, C., 1990. Thermal forcing on the tropical Pacific from satellite data. *Journal of Geophysical Research*, **95**, 13209–13217.

Liu, W. T., and Katsaros, K. B., 2001. Air-sea flux from satellite data. In Siedler, G., Church, J., and Gould, J. (eds.), *Ocean Circulation and Climate*. New York: Academic, pp. 173–1179. Ch. 3.4.

Liu, W. T., and Niiler, P. P., 1984. Determination of monthly mean humidity in the atmospheric surface layer over oceans from satellite data. *Journal of Physical Oceanography*, **14**, 1451–1457.

Liu, W. T., and Tang, W., 2005. Estimating moisture transport over ocean using spacebased observations from space. *Journal of Geophysical Research*, **110**, D10101, doi:10.1029/2004JD005300.

Liu, W. T., Tang, W., and Niiler, P. P., 1991. Humidity profiles over ocean. *Journal of Climate*, **4**, 1023–1034.

Liu, W. T., Zheng, A., and Bishop, J., 1994. Evaporation and solar irradiance as regulators of the seasonal and interannual variabilities of sea surface temperature. *Journal of Geophysical Research*, **99**, 12623–12637.

Liu, W. T., Xie, X., Tang, W., and Zlotnicki, V., 2006. Spacebased observations of oceanic influence on the annual variation of South American water balance. *Geophysical Research Letters*, **33**, L08710, doi:10.1029/2006GL025683.

Miller, D. K., and Katsaros, K. B., 1991. Satellite-derived surface latent heat fluxes in a rapidly intensifying marine cyclone. *Monthly Weather Review*, **120**, 1093–1107.

Niiler, P., 2001. The world ocean surface circulation. In Siedler, G., Gould, J., and Church, J. (eds.), *Ocean Circulation and Climate-Observing and Modeling the Global Ocean*. London: Academic, pp. 193–204.

Rienecker, M. M., et al., 2011. MERRA: NASA's modern-era retrospective analysis for research and applications. *Journal of Climate*, **24**, 3624–3648.

Roberts, B., Clayson, C. A., Robertson, F. R., and Jackson, D., 2010. Predicting near-surface atmospheric variables from SSM/I using neural networks with a first guess approach. *Journal of Geophysical Research*, **115**, D19113, doi:10.1029/2009JD013099.

Santorelli, A., Pinker, R. T., Bentamy, A., Katsaros, K. B., Drennan, W. M., Mestas-Nuñez, A. M., and Carton, J. A., 2011. Differences between two estimates of air-sea turbulent heat fluxes over the Atlantic Ocean. *Journal of Geophysical Research*, **116**, C09028, doi:10.1029/2010JC006927.

Schlüssel, P., Schanz, L., and Englisch, G., 1995. Retrieval of latent heat flux and longwave irradiance at the sea surface from SSM/I and AVHRR measurements. *Advances in Space Research*, **16**, 107–116, doi:10.1016/0273-1177(95)00389-V.

Schulz, J., Meywerk, J., Ewald, S., and Schlüssel, P., 1997. Evaluation of satellite-derived latent heat fluxes. *Journal of Climate*, **10**, 2782–2795.

Smith, S. R., Hughes, P. J., and Bourassa, M. A., 2011. A comparison of nine monthly air-sea flux products. *International Journal of Climatology*, **3**, 1002–1027, doi:10.1002/joc.2225.

Wagner, D., Ruprecht, E., and Simmer, C., 1990. A combination of microwave observations from satellite and an EOF analysis to retrieve vertical humidity profiles over the ocean. *Journal of Applied Meteorology*, **29**, 1142–1157.

WCRP, 1982. *Report of JSC/CCCO 'Cage' Experiment: A Feasibility Study.* Geneva: World Climate Research Program/World Meteorological Organization.

WCRP, 1983. *Report of the WMO/CAS Expert Meeting on Atmospheric Boundary, Parameterization Over the Oceans for Long Range Forecasting and Climate Models*. Geneva: World Climate Research Program/World Meteorological Organization.

Wentz, F.J., and Meissner, T., 2000. AMSR Ocean Algorithm, Version 2, Report number 121599A-1. Remote Sensing Systems, Santa Rosa, CA, pp. 66.

Xie, X., Liu, W. T., and Tang, B., 2008. Spacebased estimation of moisture transport in marine atmosphere using support vector machine. *Remote Sensing of Environment*, **112**, 1846–1855.

Yu, L., and Weller, R. A., 2007. Objectively analyzed air-sea heat fluxes (OAFlux) for the global ice-free oceans. *Bulletin of the American Meteorological Society*, **88**, 527–539.

OPERATIONAL TRANSITION

Richard Anthes
University Corporation for Atmospheric Research, Boulder, CO, USA

Synonyms

Research to operations; Technology transfer

Definition

Operational transition is the end-to-end set of processes that lead to the successful development and implementation of a research idea, technology, or observation in an ongoing and useful application (operations). An example is the use of atmospheric observations in daily weather forecasts, which have many applications of benefit to society.